


Suppressing classical noise in the accelerated geometric phase gate by optimized dynamical decoupling

Da-tong Chen  and Jun Jing **School of Physics, Zhejiang University, Hangzhou 310027, Zhejiang, China* (Received 4 June 2022; accepted 22 July 2022; published 3 August 2022)

In the quantum-computation scenario, the geometric phase gates are becoming increasingly attractive for their intrinsic fault tolerance to disturbance. With an adiabatic cyclic evolution, Berry phase appears to realize a geometric transformation. Performing the quantum gates as many as possible within the timescale of coherence, however, remains an inconvenient bottleneck due to the systematic errors. Here we propose an accelerated adiabatic quantum gate based on the Berry phase, the transitionless driving, and the dynamical decoupling. It reconciles a high fidelity with a high speed in the presence of control noise or imperfection. We optimize the dynamical-decoupling sequence in the time domain under a popular Gaussian noise spectrum following the inversely quadratic power law.

DOI: [10.1103/PhysRevA.106.022603](https://doi.org/10.1103/PhysRevA.106.022603)

I. INTRODUCTION

By processing the data in a quantum-mechanical way, quantum computation outperforms its classical counterpart in selected algorithms or tasks [1,2]. The simulation of the coherent evolution of generic quantum systems can be modeled by performing ordered sequences of high-fidelity unitary operations [3–5]. The ubiquitous noises from uncontrollable environment and imprecise control, however, are inevitable in any experimental proposal, which pose challenges to the quality of quantum gate in terms of fidelity and operation time [6,7]. The quantum geometric phase [8–12], which is accumulated as the system is moving along the parametric path, has intrinsic tolerant property against certain fluctuations during the trajectory. The geometric quantum computation is therefore appealing and becoming feasible in many experimental platforms, including the trapped ions [13,14], the nuclear magnetic resonance [15,16], and the superconducting circuits [17–20].

As a benchmark implementation of the Abelian geometric transformation, the quantum gate based on the Berry phase requires the quantum system to undergo a desired adiabatic loop in the parametric space [8]. The process is intrinsically slow. Reducing the evolution time is in practice demanded to avoid the accumulation of the decoherence influence. On the other hand, however, speeding up always gives rise to the transition among the instantaneous eigenstates of the system, which is supposed to be “frozen” in the adiabatic condition to maintain the gate fidelity, so that the competitive coherence time and the high fidelity are seemingly contradictory for the adiabatic geometric quantum gates. One of the compromise solutions to reduce the evolution time is using the quantum gates based on the Aharonov-Anandan phase [9,21], which emerges in arbitrary cyclic unitary evolutions. Alternatively,

one can accelerate the evolution process via the transitionless quantum driving (TQD) [22], which is formulated by the ancillary Hamiltonian to avoid the level crossing during the time evolution.

The TQD-accelerated quantum gate based on the Berry phase is still sensitive to the systematic errors in the control Hamiltonian or driving parameters. A significant feature of geometric quantum computation is its compatibility with certain error-suppression techniques, e.g., the dynamical decoupling (DD) [23–27], the unconventional geometric gates [28–30], the decoherence-free subspaces [31], the quantum error correction [32,33], and the dynamical correction [19,20], to maintain the fidelity of the adiabatic or nonadiabatic unitary transformation. The dynamical decoupling was originated in the high-precision magnetic resonance spectroscopy and has been applied to quantum control as a long-standing technique. A typical DD is to neutralize the effects from the fluctuation noises by applying a sequence of inverse operations to a two-level system [23]. In this work, we aim to find an optimized dynamical-decoupling sequence to protect the TQD-accelerated Berry-phase gate.

Particularly, we consider the effect from the Gaussian stochastic noises [34] in the control parameters of our nonadiabatic geometric quantum gates, which would deviate the output states from the noise-free result. Under various resource of noises, we analyze the robustness of the gate fidelity for a general input state to estimate the deviation and then apply the dynamical-decoupling sequences to improve the fidelity. In the time domain, we analytically derive an optimized DD sequence under the Gaussian color noise following the inversely quadratic power-law spectrum.

The rest of the work is arranged as follows. In Sec. II, we start from a semiclassical Rabi model under parametric driving and obtain a general time-dependent qubit Hamiltonian corrected by the counter-rotating interaction up to the first order. This Hamiltonian is used to establish a set of more accurate Berry-phase gates accelerated by the transitionless

*jingjun@zju.edu.cn

quantum driving. In Sec. III, we consider the stochastic fluctuations in various control parameters and their damages to the fidelity of the preceding nonadiabatic transformation in the free induction decay (FID). Then in Sec. IV, we apply the DD technique to the Berry-phase gate and discuss the results under the inversely quadratic noise spectrum. The detailed derivation of the optimized control sequence can be found in the Appendix. We discuss and summarize the whole work in Sec. V.

II. A MORE ACCURATE EFFECTIVE HAMILTONIAN

We start with a Rabi model under parametric driving, in which a two-level system (qubit) with energy-spacing ω_a is controlled by a driving field with time-modulated frequency $\omega_b(t)$ and phase factor $\varphi_R(t)$. The strength of the dipole-dipole interaction between the qubit and the driving field (Rabi frequency) is described by $\Omega_R(t)$. The system Hamiltonian thus can be written as

$$H(t) = \frac{\omega_a}{2}\sigma_z + \Omega_R(t) \cos[\Omega_b(t) + \varphi_R(t)]\sigma_x, \quad (1)$$

where $\Omega_b(t) \equiv \int_0^t ds \omega_b(s)$. It is not convenient to construct a credible quantum gate directly from the original Hamiltonian in Eq. (1) for the lack of a compact expression of the time evolution operator. It is popular to see the application of the rotating-wave approximation (RWA) in the previous treatments [14,35,36]. With respect to the unitary transformation $R(t) = \exp[i\Omega_b(t)\sigma_z/2]$, one can find

$$\begin{aligned} H'(t) &= R(t)H(t)R^\dagger(t) + i\dot{R}(t)R^\dagger(t) \\ &= \frac{1}{2}\{[\omega_a - \omega_b(t)]\sigma_z + \Omega_R(t)\{\cos\varphi_R(t) \\ &\quad + \cos[2\Omega_b(t) + \varphi_R(t)]\}\sigma_x + \Omega_R(t)\{\sin\varphi_R(t) \\ &\quad - \sin[2\Omega_b(t) + \varphi_R(t)]\}\sigma_y\} \\ &\approx \frac{\omega_a - \omega_b(t)}{2}\sigma_z + \frac{\Omega_R(t)}{2}[e^{-i\varphi_R(t)}\sigma_+ + \text{H.c.}], \end{aligned} \quad (2)$$

where the terms with the high-frequency $2\Omega_b(t)$ are omitted. The error between the resultant Hamiltonian under RWA and the original one is thus in the first order of $O(\Omega_R)$. $H'(t)$ applies to the dispersive regime of a sufficiently weak driving strength. The contribution of the omitted counter-rotating terms becomes, however, significant in the strong-coupling regime and demonstrates intriguing dynamical behaviors [37–40].

To retain the first-order contribution from the counter-rotating terms, we choose a different approach with a modified rotating-wave approximation [39]. We come back to the Hamiltonian in Eq. (1) and apply a unitary transformation with respect to

$$S(t) = \exp\left\{i\frac{\Omega_R(t)}{\omega_a + \omega_b(t)} \sin[\Omega_b(t) + \varphi_R(t)]\sigma_x\right\}. \quad (3)$$

The original Hamiltonian in the interaction picture is then rewritten as

$$\begin{aligned} H_0(t) &= S(t)H(t)S^\dagger(t) + i\dot{S}(t)S^\dagger(t) \\ &= \frac{\omega_a}{2}\sigma_z + \Omega_R(t) \cos[\Omega_b(t) + \varphi_R(t)]\sigma_x \\ &\quad + \frac{\Omega_R(t)\omega_a}{\omega_a + \omega_b(t)} \sin[\Omega_b(t) + \varphi_R(t)]\sigma_y + O(\Omega_R^2) \\ &\quad - \frac{d}{dt} \left\{ \frac{\Omega_R(t)}{\omega_a + \omega_b(t)} \sin[\Omega_b(t) + \varphi_R(t)]\sigma_x \right\} \\ &\approx \frac{\omega_a}{2}\sigma_z + \frac{\Omega_R(t)\omega_a}{\omega_a + \omega_b(t)} [e^{-i\Omega_b(t) - i\varphi_R(t)}\sigma_+ + \text{H.c.}], \end{aligned} \quad (4)$$

where we omitted the contribution up to the second order of $O(\Omega_R^2)$ and the first-order derivative of the driving parameters with respect to time [14,36] under the assumptions that $|\dot{\omega}_b(t)|$, $|\dot{\varphi}_R(t)|$, and $|\dot{\Omega}_R(t)| \ll |\omega_a + \omega_b(t)|$.

Subsequently, in the rotating frame with respect to $R(t)$, one can find a standard time-modulated Hamiltonian describing a qubit under an effective three-dimensional magnetic field, i.e.,

$$\begin{aligned} H_1(t) &= R(t)H_0(t)R^\dagger(t) + i\dot{R}(t)R^\dagger(t) \\ &= \frac{\vec{B}(t)}{2} \cdot \vec{\sigma} = \frac{B_0(t)}{2} \vec{n}(t) \cdot \vec{\sigma}, \end{aligned} \quad (5)$$

where $\vec{n}(t) \equiv [\sin\theta(t)\cos\phi(t), \sin\theta(t)\sin\phi(t), \cos\theta(t)]$ parametrizes the direction of the magnetic field and $\vec{\sigma}$ represents the vector of Pauli operators. Using the driving parameters, we have

$$\begin{aligned} B_0(t) &= \sqrt{[\omega_a - \omega_b(t)]^2 + \left[\frac{2\Omega_R(t)\omega_a}{\omega_a + \omega_b(t)}\right]^2}, \\ \phi(t) &= \varphi_R(t), \\ \theta(t) &= \arctan\left[\frac{2\Omega_R(t)\omega_a}{\omega_a^2 - \omega_b^2(t)}\right]. \end{aligned} \quad (6)$$

The Hamiltonian in Eq. (5) adapts to a larger Rabi frequency Ω_R than that in Eq. (2) by holding the first-order contribution from the counter-rotating interaction. The distinction between these two approximated Hamiltonians can be transparently illustrated by the Rabi oscillation of the population on the state $|+\rangle \equiv (1, 0)^T$ for a two-level system, when the magnitudes of ω_a , ω_b , and Ω_R are chosen in almost the same order. The blue solid line, the yellow dashed line, and the green dot-dashed line in Fig. 1 represent the respective results under the original Hamiltonian $H(t)$ in Eq. (1), the RWA Hamiltonian $H'(t)$ in Eq. (2), and the modified-RWA Hamiltonian $H_1(t)$ in Eq. (5). Much to our anticipation, the rotating-wave interaction captures the sinusoid behavior in quality, while losing nearly all the details of the dynamics. In contrast, with the aid of the unitary transformation $S(t)$ in Eq. (3), the analytical result by $H_1(t)$ is very close to the numerical one by the original Hamiltonian $H(t)$.

We then apply the effective Hamiltonian $H_1(t)$ to build a more accurate quantum gate than $H'(t)$. Universal single-qubit gates can be implemented by virtue of the time-dependent $\theta(t)$ and $\phi(t)$ in Eq. (6). B_0 is set as a constant number for simplicity. To avoid the undesired transition

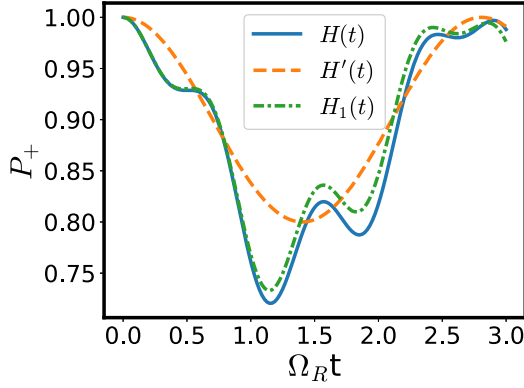


FIG. 1. The population dynamics of the qubit on $|+\rangle$ under various Hamiltonians, in units of the Rabi frequency Ω_R . The parameters are set as $\omega_a = 100\pi$ MHz, $\omega_b = 60\pi$ MHz, and $\Omega_R = 20\pi$ MHz.

among the instantaneous eigenstates of $H_1(t)$ with accelerated time dependence, one can add a counterdiabatic term following the transitionless quantum driving [22] approach. The ancillary Hamiltonian $H_{CD}(t)$ can be expressed by

$$\begin{aligned} H_{CD}(t) &= \frac{1}{2}[\dot{\vec{n}}(t) \times \vec{n}(t)] \cdot \vec{\sigma} \\ &= \frac{1}{2}(-\dot{\theta} \sin \phi - \dot{\phi} \sin \theta \cos \theta \cos \phi, \\ &\quad \dot{\theta} \cos \phi - \dot{\phi} \sin \theta \cos \theta \sin \phi, \dot{\phi} \sin^2 \theta) \cdot \vec{\sigma}, \end{aligned} \quad (7)$$

where $\vec{n}(t)$ is the unit vector of the magnetic field in Eq. (5). In Eq. (7), the explicit t dependence of quantities has been omitted for simplicity, i.e., $\theta \equiv \theta(t)$ and $\phi \equiv \phi(t)$. The corrected Hamiltonian with the counterdiabatic term is $H_{\text{tot}}(t) = H_1(t) + H_{CD}(t)$, which could be diagonalized with the unitary transformation $U_0(t) = \exp(i\theta\sigma_y/2)\exp(i\phi\sigma_z/2)$:

$$\begin{aligned} H_z(t) &= U_0(t)H_{\text{tot}}(t)U_0^\dagger(t) + i\dot{U}_0(t)U_0^\dagger(t) \\ &= \frac{1}{2}(B_0 - \dot{\phi} \cos \theta)\sigma_z. \end{aligned} \quad (8)$$

Rotating back to the concatenated rotating frame with respect to $S(t)$ and $R(t)$, where $H_1(t)$ and $H_{\text{tot}}(t)$ live, the time-evolution operator reads

$$\begin{aligned} U(t) &= U_0^\dagger(t)U_z(t) = e^{-i\phi\sigma_z/2}e^{-i\theta\sigma_y/2}e^{-i\int_0^t ds H_z(s)} \\ &= \begin{pmatrix} \cos \frac{\theta(t)}{2} e^{-(i/2)[\alpha(t)+\phi(t)]} & -\sin \frac{\theta(t)}{2} e^{(i/2)[\alpha(t)-\phi(t)]} \\ \sin \frac{\theta(t)}{2} e^{-(i/2)[\alpha(t)-\phi(t)]} & \cos \frac{\theta(t)}{2} e^{(i/2)[\alpha(t)+\phi(t)]} \end{pmatrix} \end{aligned} \quad (9)$$

with $U_z(t) \equiv \exp[-i\int_0^t ds H_z(s)]$ and $\alpha(t) = \int_0^t ds (B_0 - \dot{\phi} \cos \theta)$. Under a proper boundary condition, $U(t)$ can be used to realize any desired rotation or qubit gate. For example, under the setting that $\theta(T) = \pi$ and $\alpha(T) - \phi(T) = \pi$, $U(T)$ realizes a Pauli- X gate up to a global phase. In the following discussion, we are concerned with the phase shift in a cyclic evolution. With $\theta(T) = 2\pi$, the final time-evolution operator is found to be in a diagonal form:

$$U(T) = \begin{pmatrix} e^{-(i/2)[\alpha(T)+\phi(T)]} & 0 \\ 0 & e^{(i/2)[\alpha(T)+\phi(T)]} \end{pmatrix}, \quad (10)$$

up to an unobservable global π phase. In particular, when $|\psi(0)\rangle = |\pm\rangle [|- \rangle \equiv (0, 1)^T]$, one can derive a cyclic process

$|\psi(T)\rangle = e^{i\pi \mp (i/2)[\alpha(T)+\phi(T)]} |\psi(0)\rangle = e^{i(\pi+\gamma_\pm)} |\psi(0)\rangle$. The total phase accumulated in this period is

$$\gamma_\pm = \mp \frac{1}{2} \int_0^T dt [B_0 - \dot{\phi}(\cos \theta - 1)]. \quad (11)$$

The dynamical phase could be obtained by the corrected Hamiltonian $H_{\text{tot}}(t)$ and the eigenstates of the effective Hamiltonian $H_1(t)$. We have

$$\begin{aligned} \gamma_\pm^d &\equiv - \int_0^T dt \langle \psi(t) | H_{\text{tot}}(t) | \psi(t) \rangle \\ &= - \int_0^T dt \langle \pm | U_0(t) H_{\text{tot}}(t) U_0^\dagger(t) | \pm \rangle \\ &= - \int_0^T dt \langle \pm | \frac{1}{2} (-\dot{\phi} \sin \theta \sigma_x + \dot{\theta} \sigma_y + B_0 \sigma_z) | \pm \rangle \\ &= \mp \frac{1}{2} \int_0^T dt B_0 = \mp \frac{1}{2} B_0 T. \end{aligned} \quad (12)$$

The geometric phase is thus given by

$$\gamma_\pm^g = \gamma_\pm - \gamma_\pm^d = \mp \frac{1}{2} \int_0^T dt \dot{\phi} (1 - \cos \theta), \quad (13)$$

which is exactly the solid angle in the Bloch sphere described by θ and ϕ up to a scale of $-1/2$ [41]. The evolution period T could be shortened by TQD as long as the boundary conditions are satisfied.

Provided that the dynamical phase is completely canceled by any control technique, such as the dynamical decoupling [21,42] to be discussed later, the geometric phase in Eq. (13) determines the final time-evolution operator:

$$U(T) \simeq \begin{pmatrix} e^{i\gamma_+^g} & 0 \\ 0 & e^{i\gamma_-^g} \end{pmatrix} \simeq \begin{pmatrix} 1 & 0 \\ 0 & e^{i\int_0^T dt \dot{\phi}(1-\cos\theta)} \end{pmatrix}. \quad (14)$$

Then we can build a quantum geometric phase gate. Under the assumption $\theta(t) = \omega t$, the period is $T = 2\pi/\omega$ and $U(t) = \text{diag}\{1, e^{i\eta}\}$, where $\eta = \gamma_-^g - \gamma_+^g$. An arbitrary phase gate could be attained by adjusting ϕ . For example, we can have a Pauli- Z gate when $\phi = \omega t/2$ and we have a $\pi/2$ gate when $\phi = \omega t/4$. In general, an arbitrary input state $|\psi(0)\rangle = \cos \alpha_1 |+\rangle + \sin \alpha_1 e^{i\alpha_2} |-\rangle$ would be transformed by the phase gate to

$$|\psi(T)\rangle = \cos \alpha_1 |+\rangle + \sin \alpha_1 e^{i\alpha_2} e^{i\eta} |-\rangle, \quad (15)$$

where α_1 and α_2 are real-number angles with $\{\alpha_1, \alpha_2\} \in [0, 2\pi]$.

III. THE EFFECTS FROM CLASSICAL NOISE

The geometric evolution in Eq. (15), which has been accelerated by the counterdiabatic term, cannot be faithful in the presence of nonideal driving. The existence of the classical noise gives rise to the deviation of the gate fidelity. Here we demonstrate how the noises in various control parameters would be detrimental to the performance of quantum gates in the absence of dynamical decoupling. Then in this section, we temporarily include the dynamical phase in Eq. (12) that is exclusively determined by B_0 . The phase $\eta = \gamma_-^g - \gamma_+^g$ in

Eq. (15) then becomes $\eta = \gamma_- - \gamma_+$, i.e.,

$$\eta = \int_0^T dt [B_0 - \dot{\phi}(\cos \theta - 1)]. \quad (16)$$

To measure the phase deviation induced by the classical noise on the quantum gate, we use a gate fidelity [27,43,44] defined as

$$\mathcal{F} = \frac{1}{4\pi^2} \int_0^{2\pi} d\alpha_1 \int_0^{2\pi} d\alpha_2 \frac{M[\langle +|\rho(T)|- \rangle]}{\langle +|\psi(T)\rangle \langle \psi(T)|- \rangle}, \quad (17)$$

where $\rho(t)$ is the density matrix under the time-evolution operator $U(t)$ with noisy parameters and the wave function $|\psi(T)\rangle$ describes the ideal evolution in Eq. (15). $M[\cdot]$ means the ensemble average over the random realizations of fluctuated control parameters, e.g., $B_0 \rightarrow B_0 + \delta_B(t)$ and the arbitrary input states featured with α_1 and α_2 .

In this work, the stationary Gaussian noise [27,45] $\delta_\xi(t)$ is assumed to follow the statistical properties

$$\langle \delta_\xi(t) \rangle = 0, \quad C(t-s) = \langle \delta_\xi(t) \delta_\xi(s) \rangle = \frac{\Gamma\gamma}{2} e^{-\gamma|t-s|}, \quad (18)$$

where ξ indicates the noise source, Γ is the correlation intensity of the noise, and γ is the memory parameter. The Fourier transform of the two-point correlation function $C(t-s)$ gives rise to an inverse-quadratic spectral density,

$$S(\omega) = \int_{-\infty}^{\infty} dt e^{i\omega t} C(t) = \frac{2\Gamma\gamma^2}{\omega^2 + \gamma^2}. \quad (19)$$

When $\gamma \rightarrow \infty$, $S(\omega)$ becomes structureless and describes a Markovian or white noise; while when $\gamma \rightarrow 0$, it describes a typical non-Markovian noise with a finite-memory capability.

In the rest of this section, we calculate the gate fidelity during the free induction decay under the parametric fluctuations associated respectively with the magnetic field intensity B_0 and the phase derivative $\dot{\phi}$. Note these two parameters are separable in the expression of quantum phases, allowing individual addressing over different noise resources. In comparison to both B_0 and $\dot{\phi}$, θ comes into the phase in a cosine function [see, e.g., Eq. (16)], yielding a higher-order contribution. Thus the effect from noisy θ could be omitted.

A. Fidelity under noisy magnetic field intensity

We first consider a fluctuated magnetic field B_0 in constructing the phase gate, which is determined by the driving parameters in Eq. (5). With respect to the unitary transformation $U_0(t)$, the nonideal counterdiabatic corrected Hamiltonian in Eq. (8) becomes

$$\tilde{H}_z(t) = \frac{1}{2}[B_0 + \delta_B(t) - \dot{\phi} \cos \theta] \sigma_z. \quad (20)$$

Consequently, the off-diagonal term of the final density matrix in Eq. (17) can be obtained by

$$\langle +|\rho(T)|- \rangle = \langle +|\tilde{U}^\dagger(T)\rho(0)\tilde{U}(T)|- \rangle, \quad (21)$$

where $\rho(0) \equiv |\psi(0)\rangle \langle \psi(0)|$ and $\tilde{U}(T)$ is

$$\tilde{U}(T) = e^{-i\phi(T)\sigma_z/2} e^{-i\theta(T)\sigma_y/2} e^{-i\int_0^T ds \tilde{H}_z(s)}. \quad (22)$$

Then we have

$$\frac{\langle +|\rho(T)|- \rangle}{\langle +|\psi(T)\rangle \langle \psi(T)|- \rangle} = \exp \left[-i \int_0^T dt \delta_B(t) \right]. \quad (23)$$

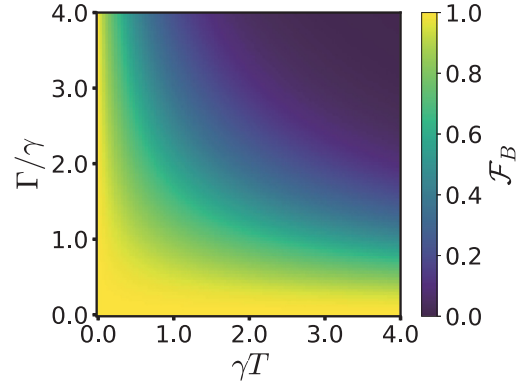


FIG. 2. Landscape of the gate fidelity \mathcal{F}_B under the stochastic B_0 in the parameter space of the strength-memory ratio Γ/γ and the running period γT .

Note this result is independent of α_1 and α_2 , meaning the noise effect on the gate fidelity does not rely on the input states. Substituting it into Eq. (17) and using the statistical properties in Eq. (18), we have [34]

$$\mathcal{F}_B = e^{-(1/2) \int_0^T dt \int_0^T ds C(t-s)} = e^{-(\Gamma/2\gamma)(\gamma T + e^{-\gamma T} - 1)}. \quad (24)$$

The dependence of the gate fidelity \mathcal{F}_B on the dimensionless cyclic period γT and the memory parameter Γ/γ is plotted in Fig. 2.

From both Eq. (24) and Fig. 2, a sufficiently large Γ/γ or a sufficiently small γ gives rise to a nearly exponential decay, which is consistent with a typical Markovian dynamics describing decoherence induced by the white noise. The nonexponential decay appears in the short-time regime with $\gamma T \ll 1$, where up to the leading order the exponent of the fidelity in Eq. (24) becomes quadratic to the running time:

$$\mathcal{F}_B \approx \exp \left(-\frac{\Gamma\gamma}{4} T^2 \right). \quad (25)$$

Then the characteristic decoherence time T_2 can be obtained by the definition $\ln \mathcal{F}_B(T_2) = -1$ [43],

$$T_2 = \frac{2}{(\Gamma\gamma)^{1/2}} \quad (26)$$

for the free induction decay. Clearly a high-level gate fidelity can be maintained in the presence of a weak and non-Markovian classical noise. It is found when $\Gamma/\gamma \leq 1.0$, \mathcal{F}_B is over 0.90 at $\gamma T = 0.72$.

B. Fidelity under noisy control phase ϕ

Now we consider the imperfect control over the phase ϕ in the presence of random noise associated with its time derivative $\dot{\phi}$, which leads to $\phi(T) \rightarrow \phi(T) + \Delta_\phi(T)$ with $\Delta_\phi(T) = \int_0^T dt \delta_\phi(t)$. Then in the rotating frame, the nonideal Hamiltonian for the accelerated phase gate becomes

$$\tilde{H}_z(t) = \frac{1}{2}[B_0 - [\dot{\phi} + \delta_\phi(t)] \cos \theta] \sigma_z. \quad (27)$$

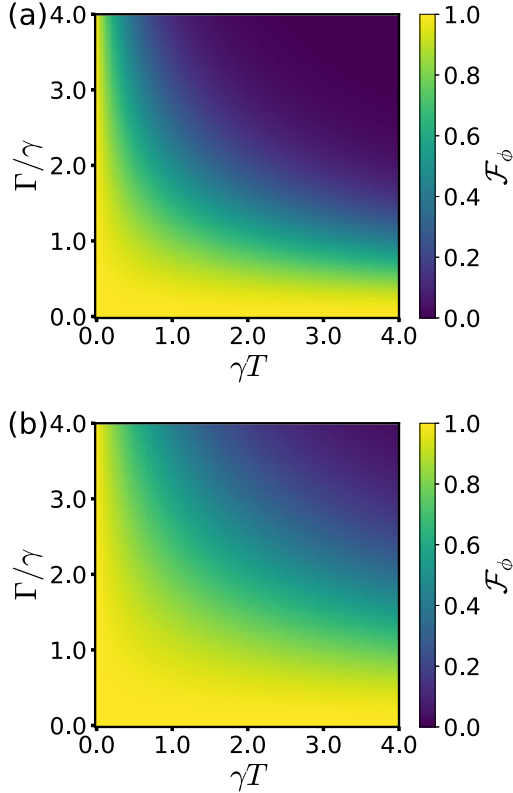


FIG. 3. Landscape of the gate fidelity \mathcal{F}_ϕ under the stochastic ϕ in the parameter space of the strength-memory ratio Γ/γ and the running period γT . In (a) and (b), the noise-free parameter θ is set as $\theta(t) = \omega t$ and $\theta(t) = \omega t - \sin(\omega t)$, respectively.

Using Eqs. (17), (21), and (27), it is straightforward to find for $\theta = \omega t$ that

$$\begin{aligned} \mathcal{F}_\phi &= e^{-(1/2) \int_0^T dt \int_0^T ds [1 - \cos \theta(t)][1 - \cos \theta(s)] C(t-s)} \\ &= \exp \left\{ - \frac{\Gamma}{4\gamma(4\pi^2 + \gamma^2 T^2)^2} [32\pi^4 e^{-\gamma T} \right. \\ &\quad \left. + 32\pi^4(-1 + \gamma T) + 20\pi^2(\gamma T)^3 + 3(\gamma T)^5] \right\}. \end{aligned} \quad (28)$$

Similar to \mathcal{F}_B in Eq. (24), the fidelity \mathcal{F}_ϕ in Eq. (28) is also a function of dimensionless parameters γT and Γ/γ . An interesting observation is that under the short-time limit, i.e., $\gamma T \ll 1$, we have $\mathcal{F}_\phi \approx \exp(-\Gamma\gamma T^2/4)$, the same as Eq. (25). Then we obtain the same decoherence timescale T_2 as in Eq. (26). One can hardly distinguish Fig. 2 and Fig. 3(a). It is found when $\Gamma/\gamma \leq 1.0$, \mathcal{F}_ϕ is over 0.90 at $\gamma T = 0.69$.

Equation (28) is, however, reminiscent of an improved scheme in constructing the quantum phase gate by virtue of the time dependence of θ . Rather than a constant θ used in literature [21,42], one can reduce the magnitude of the integrand in Eq. (28) by selecting a proper and experimentally accessible $\theta(t)$, provided that the boundary condition is satisfied. For the exponent of the fidelity in Eq. (28), the main contribution to the integral is around $t - s \approx 0$ according to the exponential decay of the correlation function $C(t - s)$ [see, e.g., Eq. (18), and the monotonic or asymptotic decay

behavior is popular for all the stationary Gaussian noises]. Then we have $\mathcal{F}_\phi \approx \exp\{-1/2(\int_0^T dt [1 - \cos \theta(t)])^2\}$. The fidelity can thus be enhanced to a certain extent by reducing the magnitude of $\int_0^T dt [1 - \cos \theta(t)]$. For example, one can replace $\theta(t) = \omega t$ with $\theta(t) = \omega t - \sin(\omega t)$ that holds the same boundary condition. The induced improvement in gate fidelity can be observed in Fig. 3(b). In contrast to Fig. 3(a), \mathcal{F}_ϕ is over 0.90 with $\Gamma/\gamma = 3.1$ when $\gamma T = 0.69$. And when $\Gamma/\gamma = 1.0$, the same high-level fidelity can be sustained until $\gamma T = 1.24$.

IV. SUPPRESS NOISE BY DYNAMICAL DECOUPLING

The noise analysis over both δ_B and δ_ϕ renders the same second-order behavior in the running time under the short-time limit, as suggested by Eqs. (25) and (26). The gate-fidelity decay induced by the classical noise on the control parameters can be suppressed by a sequence of dynamical decoupling. As a developed technique, dynamical decoupling can extend the coherence time in many experiments. It has been generalized into various sequences of pulse to neutralize the influence of the environmental noises [46]. Spin echo (SE) [47] presents the simplest yet the original form in these pulse sequences, which consists of only one π pulse in the middle of the time evolution besides another one performed in the end. Based on SE, the Carr-Purcell-Meiboom-Gill sequence (CPMG) [24,48,49] employs two or more π pulses. In general, the n -pulse version of CPMG [24] can be described by a sequence of $t_k = (k - 1/2)T/n$, $k = 1, 2, \dots, n$, that is obtained in the frequency domain. When the noise spectrum has a hard cutoff [26], i.e., $S(\omega) \sim \omega \Theta(\omega_c - \omega)$, where $\Theta(x)$ is the Heaviside step function [$\Theta(x) = 1$ when $x \geq 0$ and $\Theta(x) = 0$ when $x < 0$] or has an exponential-decay cutoff, i.e., $S(\omega) \sim \exp(-\omega/\omega_c)$, the Uhrig dynamical-decoupling (UDD) sequence [25] is shown to be the most efficient scheme. It can reduce the decoherence rate down to the n th order of the running time by using n nonperiodical pulses. In this section, we focus on the noise spectrum of the magnetic field $\delta_B(t)$ following the inverse-quadratic power law. It is shown that CPMG is the optimized choice instead of UDD. The analysis can be straightforwardly extended to the noisy ϕ .

A. Spin echo on geometric phase

We choose SE as a warm-up example to illustrate the DD effect on the geometric phase (Fig. 4). The other pulse sequences can be analyzed in a similar way. To focus on the sequence itself, the pulses are considered to be ideal, i.e., instantaneous and with no error [24,25]. The SE scheme is a concatenated process of two piecewise segments, i.e., $0 \rightarrow t_f$ and $t_f \rightarrow T$, where $t_f = T/2$. A π pulse is inserted at the moment t_f to switch the signs of the eigenstates. Another π pulse is imposed on the system in the end to complete a cyclic process. Starting from the initial state $|\psi(0)\rangle = |+\rangle$ and denoting the instantaneous eigenstates as $|\pm(t)\rangle$, the whole

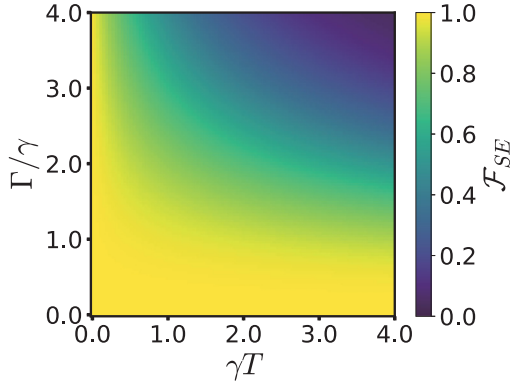


FIG. 4. Landscape of the spin-echo gate fidelity \mathcal{F}_{SE} under the stochastic B_0 in the parameter space of the strength-memory ratio Γ/γ and the running period γT .

process can be described by

$$\begin{aligned}
 |\psi(0)\rangle &= |+\rangle \rightarrow |\psi(t_f - 0^+)\rangle = e^{i\tilde{\gamma}_1} |+(t_f)\rangle \xrightarrow{\pi \text{ pulse}} \\
 |\psi(t_f + 0^+)\rangle &= e^{i\tilde{\gamma}_1} |-(t_f)\rangle \rightarrow \\
 |\psi(T - 0^+)\rangle &= e^{i(\tilde{\gamma}_1 + \tilde{\gamma}_2)} |-(T)\rangle \xrightarrow{\pi \text{ pulse}} \\
 |\psi(T)\rangle &= e^{i(\tilde{\gamma}_1 + \tilde{\gamma}_2)} |+(T)\rangle = e^{i(\pi + \tilde{\gamma}_1 + \tilde{\gamma}_2)} |+\rangle,
 \end{aligned} \tag{29}$$

where the boundary condition has been applied in the last equation. $\tilde{\gamma}_1$ and $\tilde{\gamma}_2$ represent the quantum phases generated in the first and the second segments, respectively. According to Eqs. (10), (11), and (20), these two nonideal phases turn out to be

$$\begin{aligned}
 \tilde{\gamma}_1 &= -\frac{1}{2} \int_0^{T/2} dt [B_0 + \delta_B(t) - \dot{\phi}'(\cos \theta' - 1)], \\
 \tilde{\gamma}_2 &= \frac{1}{2} \int_{T/2}^T dt [B_0 + \delta_B(t) - \dot{\phi}'(\cos \theta' - 1)],
 \end{aligned} \tag{30}$$

where $\phi' = \phi$ and $\theta' = \theta$ during the first-half period $t \in (0, t_f)$ and $\phi' = -\phi$ and $\theta' = \theta$ during the second-half period $t \in (t_f, T)$ due to the spin-echo effect. By Eq. (30), the ideal dynamical phase proportional to B_0 vanishes in the end of the running while the geometric phase is accumulated to realize a desired transformation and it holds the same form as in Eq. (13). When the initial state starts from $|\psi(0)\rangle = |-\rangle$, the signs of those phases in Eq. (30) are reversed and the SE scheme still works. In any loop, however, the dynamical phase associated with the accumulation of the stochastic noise $\delta_B(t)$ during the two consecutive time integrals has not been completely eliminated.

Then we measure the gate fidelity in the presence of the random magnetic field under the spin-echo scheme. The ratio of the off-diagonal elements of the density matrix in Eq. (17) is found to be

$$\frac{\langle +|\rho(T)|-\rangle}{\langle +|\psi(T)\rangle\langle \psi(T)|-\rangle} = e^{-i[\int_0^{T/2} dt \delta_B(t) - \int_{T/2}^T dt \delta_B(t)]}. \tag{31}$$

On ensemble average, we have

$$\begin{aligned}
 \mathcal{F}_{SE} &= M \left[\exp \left(-i \int_0^{T/2} dt \delta_B(t) + i \int_{T/2}^T dt \delta_B(t) \right) \right] \\
 &= \exp \left[-\frac{\Gamma}{2\gamma} (\gamma T - e^{-\gamma T} - 3 + 4e^{-\gamma T/2}) \right],
 \end{aligned} \tag{32}$$

as plotted in Fig. 4. In contrast to Fig. 2, one can find that under the SE scheme, the high-level regime of the gate fidelity is significantly enlarged. When $\Gamma/\gamma = 2.0$, \mathcal{F}_{SE} can be maintained over 0.98 for $\gamma T = 1.0$. In the short-time limit $\gamma T \ll 1$, we have

$$\mathcal{F}_{SE} \approx \exp \left(-\frac{\Gamma\gamma^2}{24} T^3 \right). \tag{33}$$

In comparison to the quadratic dependence in Eq. (25), the exponent function is reduced to the third order of the running time of the geometric gate by the spin-echo effect. It is shown in the Appendix that for the inversely quadratic power-law noise spectrum, one can further reduce the decay coefficient by more DD operations, yet cannot reduce the exponent function to more higher orders of the running interval T .

B. CPMG on geometric phase

Generally, we apply n π pulses into the running period $(0, T)$ to suppress the geometric-phase error. The whole process is divided into $n + 1$ segments described by $0 \rightarrow t_1, t_1 \rightarrow t_2, \dots, t_n \rightarrow T$. We then seek an optimized sequence of the DD-operation moments t_k . Similar to Eq. (32), the gate fidelity can be represented by

$$\mathcal{F}_n = M \left[e^{-i \int_0^T dt \delta_B(t) f(T;t)} \right], \tag{34}$$

where $f(T;t) = \sum_{k=0}^n (-1)^k \Theta(t_{k+1} - t) \Theta(t - t_k)$ with $t_0 = 0$ and $t_{n+1} = T$, indicating the π -pulse-induced sign change of the quantum phase. Moreover, to hold the same geometric phase as that in Eq. (13) for the FID process, the phase parameters ϕ' and θ' in all the segments are set as $\phi' = f(T;t)\phi$ and $\theta' = \theta$.

The gate fidelity in Eq. (34) can be represented by $\mathcal{F}_n \equiv e^{-\chi(T)}$ [43,44], where the decay function $\chi(T)$ is obtained by the noise spectrum $S(\omega)$ and $\tilde{f}(\omega, T) = \int_0^T dt e^{-i\omega t} f(T;t)$ [the Fourier transform of $f(T;t)$],

$$\begin{aligned}
 \chi(T) &= \frac{1}{2} \int_{-\infty}^{\infty} \frac{d\omega}{2\pi} |\tilde{f}(\omega, T)|^2 S(\omega) \\
 &= \frac{1}{2} \int_{-\infty}^{\infty} \frac{d\omega}{\pi} \frac{F(\omega T)}{\omega^2} S(\omega).
 \end{aligned} \tag{35}$$

Note in the second line of Eq. (35), a filter function $F(\omega T) \equiv |\omega \tilde{f}(\omega, T)|^2/2$ appears to measure the effects of the pulse sequence. Using the Taylor expansion around $\omega T = 0$, we have

$$\begin{aligned}
 \chi(T) &= \int_{-\infty}^{\infty} \frac{d\omega}{2\pi\omega^2} \left[F(0) + F'(0)\omega T + F''(0)\frac{(\omega T)^2}{2!} \right. \\
 &\quad \left. + F^{(3)}(0)\frac{(\omega T)^3}{3!} + \dots \right] S(\omega).
 \end{aligned} \tag{36}$$

Under the general noise with a power-law spectrum $S(\omega) \sim 1/\omega^m$, $m \geq 2$, the high-order terms $F^{(n)}(0)$ with $n - m \geq 1$

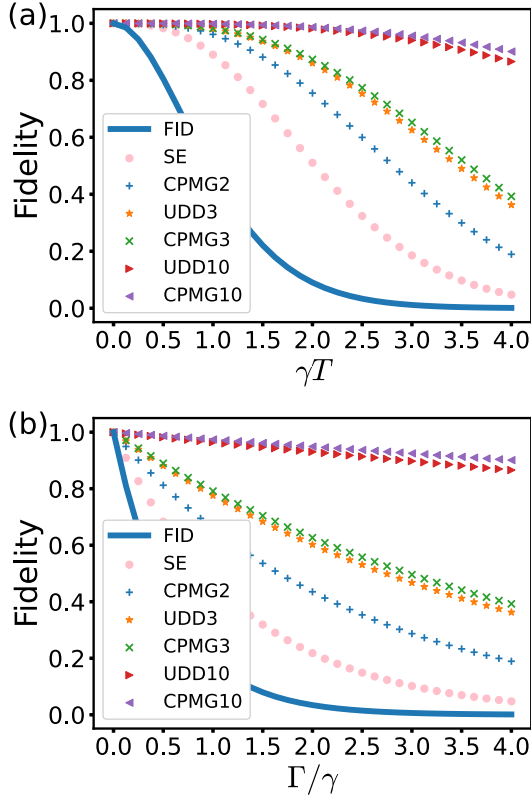


FIG. 5. The gate fidelity under various DD sequences (SE, CPMGn, and UDDn) in the presence of the Gaussian noise following the inverse-quadratic power-law spectrum. (a) The gate dynamics versus γT when $\Gamma/\gamma = 4$; (b) the gate dependence on Γ/γ when $\gamma T = 4$.

would lead to the nonconvergent integration $\int_{-\infty}^{\infty} d\omega \omega^{n-2-m}$. In contrast, if $S(\omega)$ has a hard cutoff at an upper-bound frequency ω_c or has an exponential decay with frequency, such as $S(\omega) \sim \exp(-\omega/\omega_c)$, then the convergence could be held at any order. Without frequency cutoff, the UDD scheme [25] does not necessarily supply an optimized sequence for a polynomial spectrum.

Some existing works [43,44] about DD have addressed the noise $\delta_B(t)$ with the statistical properties in Eq. (18). Here we provide an alternative way in the Appendix to optimize the pulse sequence in the time domain for the quadratic power-law spectrum. We find the most efficient sequence can be analytically described by

$$t_k = \frac{(k - 1/2)}{n} T, \quad k = 1, 2, \dots, n, \quad (37)$$

which is exactly the CPMGn sequence with $n \geq 2$. When $n = 1$, it reduces to the SE sequence. When $n = 2$, it is also coincident to the UDD sequence.

In Figs. 5(a) and 5(b), we show the gate fidelities under various DD sequences in terms of the dynamics and their dependence on the memory parameter, respectively. The solid line, circle-dotted line, plus-dotted line, star-dotted line, cross-dotted line, right-triangle-dotted line, and left-triangle-dotted line represent the fidelities under FID, SE, CPMG2, UDD3, CPMG3, UDD10, and CPMG10, respectively, where n de-

notes the number of π pulses. In both Figs. 5(a) and 5(b), the performance of the geometric phase gate is steadily improved by inserting more periodical π pulses into the running period. We also demonstrate that CPMGn outperforms UDDn when $n \geq 3$. It is found when $\Gamma/\gamma = 4.0$ and $\gamma T = 4.0$, the gate fidelity can be maintained over 0.90 by CPMG10. By Eqs. (37) and (35), it is found that up to the leading-order contribution the gate fidelity becomes

$$\mathcal{F}_n \approx \exp \left[-\frac{\Gamma}{24n^2\gamma} (\gamma T)^3 \right]. \quad (38)$$

As for the scaling of the decoherence time T_2 over the pulse number n , we have

$$T_2 = \left(\frac{24}{\Gamma\gamma^2} \right)^{1/3} n^{2/3}. \quad (39)$$

The power law with $n^{2/3}$ implies that more DD pulses are required to enhance the coherence time of our geometric phase gate.

V. DISCUSSION AND CONCLUSION

The analysis over the classical noise in this work is mainly based on the Gaussian approximation. Then the two-point correlation function $C(t - s)$ is sufficient to determine its impact on the decoherence behavior in the time evolution. As pointed out in literature [43,44], random telegraph noise in the weak noise regime can be described by Eq. (18) and the power-law noise can be described by a linear combination of the similar correlation functions with various parameters. Under the non-Gaussian assumption, the noise effect also involves a multiple-point correlation function. It is thus not convenient to analytically obtain \mathcal{F}_B in Eq. (24), \mathcal{F}_ϕ in Eq. (28), and \mathcal{F}_{SE} in Eq. (32) to witness the effect of a non-Markovian noise on the gate fidelity. Although the non-Gaussian noise would reduce the coherence time in FID, it has been shown to be more suppressed under CPMG rather than UDD [44]. The non-Gaussian noise is therefore negligible when applying our dynamical-decoupling scheme, that is proved to be a CPMG, into the accelerated phase-gate construction.

In summary, we construct a quick-and-faithful geometric phase gate by combining the transitionless-quantum-driving approach and the dynamical-decoupling control into the Berry phase. The former is used to shorten the running time as required by the adiabatic passage and the latter is used to neutralize the classical noise on the control parameters. Our proposal is based on a semiclassical Rabi model under a parametric driving. Using a modified transformation to hold the first-order contribution from the counter-rotating interaction, our effective Hamiltonian is superior to that under the conventional rotating-wave approximation and adapts to a strong driving beyond the dispersive regime. We analyze the gate fidelity under the random fluctuation or noise on the effective magnetic field and the control phase. In the time domain, we find that the CPMGn sequence is the most efficient DD scheme against the inversely quadratic power-law noise to maintain a high-level fidelity and we obtain the scaling behavior of the decoherence time T_2 with respect to the DD operation number n . Our investigation provides a systematic estimation over the errors in constructing the Berry-phase gate

caused by the classical noise. It is useful in optimizing the performance of quantum gates under Gaussian noise following a power-law spectrum.

In addition, combining the noninstantaneous DD pulses with the approximated TQD approaches [50,51] would be a near-future target. The phase-gate fidelity is supposed to be more robust when the counterdiabatic operation could be performed along the same direction as the DD pulses.

ACKNOWLEDGMENT

We acknowledge financial support from the National Science Foundation of China (Grants No. 11974311 and No. U1801661).

APPENDIX: OPTIMIZED SEQUENCE FOR GAUSSIAN NOISE OF POWER-LAW SPECTRUM

This Appendix contributes to optimizing the DD sequence to cancel the classical Gaussian noise on the magnetic-field intensity. We provide a proof in the time domain rather than that in the frequency domain [43]. The derivation starts from the gate fidelity under n pulses in Eq. (34). Using the correlation function in Eq. (18), we have

$$\begin{aligned} \mathcal{F}_n(\{t_k, k = 1, 2, \dots, n\}) &= M[e^{-i \int_0^T dt \delta_B(t) f(T; t)}] \\ &= \exp\left[-\frac{1}{2} \int_0^T dt \int_0^T ds C(t-s) f(T; t) f(T; s)\right]. \end{aligned} \quad (\text{A1})$$

With the dimensionless parameters $x \equiv \gamma T$, $y \equiv \Gamma/\gamma$, and $\mu_k \equiv t_k/T$, the decay function $\chi(x, y) \equiv -\ln \mathcal{F}_n$ can be expressed by

$$\begin{aligned} \chi(x, y) &= \frac{y}{2} \left[x - 1 + (-1)^n e^{-x} \right. \\ &\quad \left. - 2 \sum_{k=0}^{n+1} \sum_{j=1}^n (-1)^{|k-j|} e^{-|\mu_k - \mu_j|x} \right], \end{aligned} \quad (\text{A2})$$

where $\mu_0 = 0$ and $\mu_{n+1} = 1$. Note expanding $\chi(x, y)$ about x is equivalent to expanding it about T . It is obtained that

$$\chi(x, y) = \frac{y}{2} (C_0 + C_1 x + C_2 x^2 + C_3 x^3 + \dots), \quad (\text{A3})$$

where the coefficients of the first few orders are

$$C_0 = -1 + (-1)^n - 2 \sum_{k=0}^{n+1} \sum_{j=1}^n (-1)^{|k-j|}, \quad (\text{A4a})$$

$$C_1 = 1 - (-1)^n + 2 \sum_{k=0}^{n+1} \sum_{j=1}^n (-1)^{|k-j|} |\mu_k - \mu_j|, \quad (\text{A4b})$$

$$C_2 = \frac{1}{2} (-1)^n - \sum_{k=0}^{n+1} \sum_{j=1}^n (-1)^{|k-j|} |\mu_k - \mu_j|^2, \quad (\text{A4c})$$

$$C_3 = \frac{1}{6} (-1)^{n+1} + \frac{1}{3} \sum_{k=0}^{n+1} \sum_{j=1}^n (-1)^{|k-j|} |\mu_k - \mu_j|^3. \quad (\text{A4d})$$

It is straightforward to verify that both the zero-order and the first-order coefficients C_0 and C_1 are exactly 0, irrespective to the sequence arrangement $\{\mu_k\}$.

When n is an even integer, the summation in the second-order coefficient C_2 can be decomposed into three terms, being formally relevant to μ_k^2 , $-2\mu_k\mu_j$, and μ_j^2 , respectively. By virtue of $\mu_0 = 0$ and $\mu_{n+1} = 1$, the μ_k^2 or μ_j^2 term is proved to vanish by

$$\sum_{k=0}^{n+1} \sum_{j=1}^n (-1)^{|k-j|} \mu_k^2 = \sum_{k=0}^{n+1} \mu_k^2 \sum_{j=1}^n (-1)^{|k-j|} = 0. \quad (\text{A5})$$

Equation (A4c) can then be reduced to

$$\begin{aligned} C_2 &= \frac{1}{2} + 2 \sum_{k=0}^{n+1} \sum_{j=1}^n (-1)^{|k-j|} \mu_k \mu_j \\ &= \frac{1}{2} + 2 \left[\sum_{k=1}^n (-1)^{k-1} \mu_k \right]^2 + 2 \sum_{k=1}^n (-1)^{k-1} \mu_k \\ &= \frac{1}{2} \left[1 + \sum_{k=1}^n (-1)^{k-1} 2\mu_k \right]^2. \end{aligned} \quad (\text{A6})$$

When n is odd, the summations about μ_k^2 and μ_j^2 in C_2 are simplified to

$$\begin{aligned} &\sum_{k=0}^{n+1} \mu_k^2 \sum_{j=1}^n (-1)^{|k-j|} + \sum_{j=1}^n \mu_j^2 \sum_{k=0}^{n+1} (-1)^{|k-j|} \\ &= \sum_{k=0}^{n+1} \mu_k^2 (-1)^{|k-1|} + \sum_{j=1}^n \mu_j^2 (-1)^j \\ &= \mu_0^2 (-1)^1 + \mu_{n+1}^2 (-1)^n = -1. \end{aligned} \quad (\text{A7})$$

Then Eq. (A4c) can be reduced to

$$\begin{aligned} C_2 &= -\frac{1}{2} - (-1) + 2 \sum_{k=0}^{n+1} \sum_{j=1}^n (-1)^{|k-j|} \mu_k \mu_j \\ &= \frac{1}{2} + 2 \left[\sum_{k=1}^n (-1)^{k-1} \mu_k \right]^2 - 2 \sum_{k=1}^n (-1)^{k-1} \mu_k \\ &= \frac{1}{2} \left[-1 + \sum_{k=1}^n (-1)^{k-1} 2\mu_k \right]^2. \end{aligned} \quad (\text{A8})$$

Summarizing Eqs. (A6) and (A8), the condition of $C_2 = 0$ can be written as

$$(-1)^n + 2 \sum_{k=1}^n (-1)^{k-1} \mu_k = 0. \quad (\text{A9})$$

It has a clear physical indication or consequence that after applying those π pulses at μ_k , the dynamical phase in the absence of noise is thus exactly eliminated to leave a geometric transformation.

To find the optimized sequence, we now study the extreme-value condition $\partial_{\mu_k} C_3 = 0$, $k = 1, 2, \dots, n$, under the constraints that $0 < \mu_1 < \mu_2 < \dots < \mu_n < 1$. By virtue

of Eq. (A9), we have

$$\mu_n = \sum_{k=1}^{n-1} (-1)^{n-k-1} \mu_k + \frac{1}{2}. \quad (\text{A10})$$

With Eq. (A4d), we have for $k = n - 1$ that

$$\begin{aligned} \frac{\partial C_3}{\partial \mu_{n-1}} = & (\mu_{n-1} - \mu_n) \left[2 - \mu_{n-1} - \mu_n \right. \\ & \left. + (-1)^{n-1} (\mu_{n-1} + \mu_n) \right. \\ & \left. + 2 \sum_{k=1}^{n-2} (-1)^{n-k-1} (\mu_{n-1} + \mu_n - 2\mu_k) \right] = 0. \end{aligned} \quad (\text{A11})$$

For n either even or odd, it gives rise to

$$\mu_{n-1} = \frac{3}{2} \sum_{k=1}^{n-2} (-1)^{n-k-2} \mu_k + \frac{1}{4}. \quad (\text{A12})$$

By a similar derivation with decreasing k , we can obtain a general formula

$$\mu_{n-j} = \frac{2j+1}{j+1} \sum_{k=1}^{n-j-1} (-1)^{n-k-j-1} \mu_k + \frac{1}{2j+2}. \quad (\text{A13})$$

In the end, it is found that $\mu_1 = 1/(2n)$. Then by iteratively using Eq. (A13), we can find the solution is exactly the CPMG n , i.e., $\mu_k = (k - 1/2)/n$. And the minimum value of the third-order coefficient C_3 turns out to be $x^3/(12n^2)$, which corresponds to the decay behavior in Eq. (38) of the main text. The result also demonstrates that the C_3 cannot be completely eliminated under an arbitrary choice of μ_k or t_k .

-
- [1] P. W. Shor, Polynomial-time algorithms for prime factorization and discrete logarithms on a quantum computer, *SIAM J. Comput.* **26**, 1484 (1997).
- [2] L. K. Grover, Quantum Mechanics Helps in Searching for a Needle in a Haystack, *Phys. Rev. Lett.* **79**, 325 (1997).
- [3] R. Babbush, P. J. Love, and A. Aspuru-Guzik, Adiabatic quantum simulation of quantum chemistry, *Sci. Rep.* **4**, 6603 (2014).
- [4] R. Gerritsma, G. Kirchmair, F. Zähringer, E. Solano, R. Blatt, and C. Roos, Quantum simulation of the Dirac equation, *Nature (London)* **463**, 68 (2010).
- [5] I. D. Kivlichan, J. McClean, N. Wiebe, C. Gidney, A. Aspuru-Guzik, G. K.-L. Chan, and R. Babbush, Quantum Simulation of Electronic Structure with Linear Depth and Connectivity, *Phys. Rev. Lett.* **120**, 110501 (2018).
- [6] R. Harper, S. T. Flammia, and J. J. Wallman, Efficient learning of quantum noise, *Nat. Phys.* **16**, 1184 (2020).
- [7] C. Song, S.-B. Zheng, P. Zhang, K. Xu, L. Zhang, Q. Guo, W. Liu, D. Xu, H. Deng, K. Huang *et al.*, Continuous-variable geometric phase and its manipulation for quantum computation in a superconducting circuit, *Nat. Commun.* **8**, 1061 (2017).
- [8] M. V. Berry, Quantal phase factors accompanying adiabatic changes, *Proc. R. Soc. London, Ser. A* **392**, 45 (1984).
- [9] Y. Aharonov and J. Anandan, Phase Change During a Cyclic Quantum Evolution, *Phys. Rev. Lett.* **58**, 1593 (1987).
- [10] J. Samuel and R. Bhandari, General Setting for Berry's Phase, *Phys. Rev. Lett.* **60**, 2339 (1988).
- [11] F. Wilczek and A. Zee, Appearance of Gauge Structure in Simple Dynamical Systems, *Phys. Rev. Lett.* **52**, 2111 (1984).
- [12] J. Anandan, Non-adiabatic non-Abelian geometric phase, *Phys. Lett. A* **133**, 171 (1988).
- [13] D. Leibfried, B. DeMarco, V. Meyer, D. Lucas, M. Barrett, J. Britton, W. M. Itano, B. Jelenković, C. Langer, T. Rosenband *et al.*, Experimental demonstration of a robust, high-fidelity geometric two ion-qubit phase gate, *Nature (London)* **422**, 412 (2003).
- [14] J.-M. Cui, M.-Z. Ai, R. He, Z.-H. Qian, X.-K. Qin, Y.-F. Huang, Z.-W. Zhou, C.-F. Li, T. Tu, and G.-C. Guo, Experimental demonstration of suppressing residual geometric dephasing, *Sci. Bull.* **64**, 1757 (2019).
- [15] J. A. Jones, V. Vedral, A. Ekert, and G. Castagnoli, Geometric quantum computation using nuclear magnetic resonance, *Nature (London)* **403**, 869 (2000).
- [16] G. Feng, G. Xu, and G. Long, Experimental Realization of Nonadiabatic Holonomic Quantum Computation, *Phys. Rev. Lett.* **110**, 190501 (2013).
- [17] A. A. Abdumalikov, Jr., J. M. Fink, K. Juliusson, M. Pechal, S. Berger, A. Wallraff, and S. Filipp, Experimental realization of non-Abelian non-adiabatic geometric gates, *Nature (London)* **496**, 482 (2013).
- [18] Y. Xu, W. Cai, Y. Ma, X. Mu, L. Hu, T. Chen, H. Wang, Y. P. Song, Z.-Y. Xue, Z.-q. Yin, and L. Sun, Single-Loop Realization of Arbitrary Nonadiabatic Holonomic Single-Qubit Quantum Gates in a Superconducting Circuit, *Phys. Rev. Lett.* **121**, 110501 (2018).
- [19] J. Zhou, S. Li, G.-Z. Pan, G. Zhang, T. Chen, and Z.-Y. Xue, Nonadiabatic geometric quantum gates that are insensitive to qubit-frequency drifts, *Phys. Rev. A* **103**, 032609 (2021).
- [20] M.-J. Liang and Z.-Y. Xue, Robust nonadiabatic geometric quantum computation by dynamical correction, *Phys. Rev. A* **106**, 012603 (2022).
- [21] X. B. Wang and M. Keiji, Nonadiabatic Conditional Geometric Phase Shift with NMR, *Phys. Rev. Lett.* **87**, 097901 (2001).
- [22] M. V. Berry, Transitionless quantum driving, *J. Phys. A: Math. Theor.* **42**, 365303 (2009).
- [23] L. Viola and S. Lloyd, Dynamical suppression of decoherence in two-state quantum systems, *Phys. Rev. A* **58**, 2733 (1998).
- [24] W. M. Witzel and S. D. Sarma, Multiple-Pulse Coherence Enhancement of Solid State Spin Qubits, *Phys. Rev. Lett.* **98**, 077601 (2007).
- [25] G. S. Uhrig, Keeping a Quantum Bit Alive by Optimized π -Pulse Sequences, *Phys. Rev. Lett.* **98**, 100504 (2007).
- [26] S. Pasini and G. S. Uhrig, Optimized dynamical decoupling for power-law noise spectra, *Phys. Rev. A* **81**, 012309 (2010).
- [27] X.-K. Qin, G.-C. Guo, and Z.-W. Zhou, Suppressing the geometric dephasing of Berry phase by using modified dynamical decoupling sequences, *New J. Phys.* **19**, 013025 (2017).
- [28] S.-L. Zhu and Z. D. Wang, Unconventional Geometric Quantum Computation, *Phys. Rev. Lett.* **91**, 187902 (2003).

- [29] J. Du, P. Zou, and Z. D. Wang, Experimental implementation of high-fidelity unconventional geometric quantum gates using an NMR interferometer, *Phys. Rev. A* **74**, 020302 (2006).
- [30] Z. S. Wang, C. Wu, X.-L. Feng, L. C. Kwek, C. H. Lai, C. H. Oh, and V. Vedral, Nonadiabatic geometric quantum computation, *Phys. Rev. A* **76**, 044303 (2007).
- [31] X.-L. Feng, C. Wu, H. Sun, and C. H. Oh, Geometric Entangling Gates in Decoherence-Free Subspaces with Minimal Requirements, *Phys. Rev. Lett.* **103**, 200501 (2009).
- [32] O. Oreshkov, T. A. Brun, and D. A. Lidar, Fault-Tolerant Holonomic Quantum Computation, *Phys. Rev. Lett.* **102**, 070502 (2009).
- [33] O. Oreshkov, T. A. Brun, and D. A. Lidar, Scheme for fault-tolerant holonomic computation on stabilizer codes, *Phys. Rev. A* **80**, 022325 (2009).
- [34] C. Gardiner, P. Zoller, and P. Zoller, *Quantum Noise: A Handbook of Markovian and Non-Markovian Quantum Stochastic Methods with Applications to Quantum Optics* (Springer Science & Business Media, Berlin/Heidelberg, 2004)
- [35] C. Gerry, P. Knight, and P. L. Knight, *Introductory Quantum Optics* (Cambridge University Press, Cambridge, UK, 2005).
- [36] P. J. Leek, J. M. Fink, A. Blais, R. Bianchetti, M. Göppl, J. M. Gambetta, D. I. Schuster, L. Frunzio, R. J. Schoelkopf, and A. Wallraff, Observation of Berry's phase in a solid-state qubit, *Science* **318**, 1889 (2007).
- [37] H. Zheng, S. Y. Zhu, and M. S. Zubairy, Quantum Zeno and Anti-Zeno Effects: Without the Rotating-Wave Approximation, *Phys. Rev. Lett.* **101**, 200404 (2008).
- [38] C. Deng, F. Shen, S. Ashhab, and A. Lupascu, Dynamics of a two-level system under strong driving: Quantum-gate optimization based on Floquet theory, *Phys. Rev. A* **94**, 032323 (2016).
- [39] Z. Lü and H. Zheng, Effects of counter-rotating interaction on driven tunneling dynamics: Coherent destruction of tunneling and Bloch-Siegert shift, *Phys. Rev. A* **86**, 023831 (2012).
- [40] J. Jing, Z.-G. Lü, and Z. Ficek, Breakdown of the rotating-wave approximation in the description of entanglement of spin-anticorrelated states, *Phys. Rev. A* **79**, 044305 (2009).
- [41] W. Dong, F. Zhuang, S. E. Economou, and E. Barnes, Doubly geometric quantum control, *PRX Quantum* **2**, 030333 (2021).
- [42] A. Gregefalk and E. Sjöqvist, Transitionless Quantum Driving in Spin Echo, *Phys. Rev. Applied* **17**, 024012 (2022).
- [43] L. Cywiński, R. M. Lutchyn, C. P. Nave, and S. Das Sarma, How to enhance dephasing time in superconducting qubits, *Phys. Rev. B* **77**, 174509 (2008).
- [44] P. Szańkowski, G. Ramon, J. Krzywda, D. Kwiatkowski, and Ł. Cywiński, Environmental noise spectroscopy with qubits subjected to dynamical decoupling, *J. Phys.: Condens. Matter* **29**, 333001 (2017).
- [45] J. Jing, C.-H. Lam, and L.-A. Wu, Non-Abelian holonomic transformation in the presence of classical noise, *Phys. Rev. A* **95**, 012334 (2017).
- [46] W. Yang, Z.-Y. Wang, and R.-B. Liu, Preserving qubit coherence by dynamical decoupling, *Front. Phys. China* **6**, 2 (2011).
- [47] E. L. Hahn, Spin echoes, *Phys. Rev.* **80**, 580 (1950).
- [48] H. Y. Carr and E. M. Purcell, Effects of diffusion on free precession in nuclear magnetic resonance experiments, *Phys. Rev.* **94**, 630 (1954).
- [49] S. Meiboom and D. Gill, Modified spin-echo method for measuring nuclear relaxation times, *Rev. Sci. Instrum.* **29**, 688 (1958).
- [50] T. Hatomura and K. Takahashi, Controlling and exploring quantum systems by algebraic expression of adiabatic gauge potential, *Phys. Rev. A* **103**, 012220 (2021).
- [51] P. Chandarana, N. N. Hegade, K. Paul, F. Albarrán-Arriagada, E. Solano, A. del Campo, and X. Chen, Digitized-counterdiabatic quantum approximate optimization algorithm, *Phys. Rev. Research* **4**, 013141 (2022).